Water Air Soil Pollut (2013) 224:1666
DOI 10.1007/s11270-013-1666-2

Minor Losses During Air Flow into Granular Porous Media

Tjalfe G. Poulsen · Greta Minelgaite · Thomas R. Bentzen · Rune R. Andreasen

Received: 11 April 2013 / Accepted: 23 July 2013 / Published online: 13 August 2013

Abstract Pressure gradients during uniform fluid flow in porous media are traditionally assumed to be linear. Thus, pressure loss across a sample of porous medium is assumed directly proportional to the thickness of the sample. In this study, measurements of pressure gradients inside coarse granular (2–18 mm particle size) porous media during steady gas flow were carried out. The results showed that pressure variation with distance in the porous media was nonlinear near the inlet (where pressure gradients were higher) but became linear at greater distances (with a lower gradient). This indicates that the pressure loss in porous media consists of two components: (1) a linear pressure gradient and (2) an initial pressure loss near the inlet. This initial pressure loss is also known from hydraulics in tubes as a minor loss and is associated with abrupt changes in the flow field such as narrowings and bends. The results further indicated that the minor loss depends on the particle size and particle size distribution in a manner similar to that of the linear pressure gradient. There is, thus, a close relation between these two components. In porous media, the minor loss is not instantaneous at the inlet point but happens over some distance starting upstream from the inlet and ending some distance downstream.

Keywords Granular porous media · Fluid flow · Fluid pressure loss · Minor losses · Pressure gradient · Particle size distribution

1 Introduction

Growing world population and increased standard of living in many regions have created an increased demand for meat as a major component of human food intake. As a result, meat production (especially pig production) as well as the size of the production units (farms) have increased over the past decades. This has created increased emissions of airborne nutrients (ammonia) and odorous compounds (such as amines and sulfur containing compounds) which in turn have caused ecosystem damage and nuisances for the neighbors. Other sources contributing to the release of odors and airborne contaminants are wastewater treatment plants, solid waste processing facilities, composting facilities, and biogas plants as well as certain industries (Shareefdeen et al. 2005). There is therefore a need for new and reliable solutions with respect to air pollution control (Shareefdeen et al. 2005; Delhomenie and Heitz 2005).

T. G. Poulsen (✉)
Department of Civil Engineering, Xi'an Jiaotong–Liverpool University,
111 Ren Ai Rd, 215123 Suzhou, China
e-mail: tjalfe.poulsen@xjtlu.edu.cn

G. Minelgaite · T. R. Bentzen
Section for Water and Environment, Department of Civil Engineering, Aalborg University,
Sohngaardsholmsvej 57, 9000 Aalborg, Denmark

R. R. Andreasen
Department of Agroecology, Aarhus University,
Blichers Allé 20, 8830 Tjele, Denmark

Biofiltration has been demonstrated to be a potentially cost-effective technology that is simple to operate, can be applied for a wide variety of airborne pollutants, and requires much less energy compared to conventional physical or chemical air treatment systems (Revah and Morgan-Sagastume 2005). Biofilters have been demonstrated to be able to remove a wide variety of volatile compounds (Delhomenie and Heitz 2005), which are generally turned into carbon dioxide, water, and mineral salts (Datta and Allen 2005). Biofiltration is therefore, likely the most optimal, environmentally friendly and cost-effective process for the treatment of biodegradable and odorous contaminants in air (Deshusses 1997; Shareefdeen et al. 2003; Dorado et al. 2010).

Biofilter's cost-efficiency depends on both filter geometry and operation conditions (Schlegelmilch et al. 2005), as well as filter material properties (especially with respect to biofilm growth possibilities) (Schwarz et al. 2001). Operating costs are especially important in connection with livestock farms due to the often very large air volumes that must be treated (200–300 m^3h^{-1} per animal) in order to maintain proper indoor climate for the animals and to avoid negative consequences for the indoor environment (Blanes and Pedersen 2005; O'Neill et al. 1992). As filter energy consumption (and thereby operation costs) is proportional to the air flow rate and the pressure loss (ΔP) across the filter, these parameters are especially important for process economy (Yang and Allen 2005).

Generally pressure loss, ΔP, depends on the gas flow through the filter and on filter material characteristics such as particle size distribution, particle shape, and degree of biomass accumulation in the material (Schwarz et al. 2001; Delhomenie and Heitz 2005; Andreasen et al. 2012).

Several expressions for predicting steady-state pressure loss in porous materials as a function of fluid velocity and medium properties have been suggested (Darcy 1856; Forchheimer 1901; Ergun 1952; Macdonald et al. 1979; Andreasen and Poulsen 2013). These expressions generally assume that the pressure gradient across a homogeneous biofilter medium during uniform fluid flow is constant. Thus, the pressure inside the filter medium is assumed to decrease linearly with increasing filter depth. Preliminary experiments carried out in connection with this study, however, indicate that the pressure gradient inside the filter medium is not constant, especially near the filter inlet, where there is an increased pressure loss. This phenomenon was noticed to be equivalent to the changes in pressure gradient observed for fluid flow in a pipe with a bend or change in a cross sectional area, described by Munson et al. (2006) where so-called minor losses in the pressure occur. These changes have been shown to depend on fluid velocity, pipe diameter, shape of the bend, or change in the cross sectional area. Considering that the air flow in pores of a porous medium to some degree is comparable to fluid flow in pipes, it is reasonable to assume that minor losses can occur also in connection with flow into porous media. However, this phenomenon has not yet been demonstrated to occur in porous media. The implications are that for instance doubling filter depth does not necessarily mean doubling the pressure loss across the filter, an assumption that is generally applied at present.

The main objective of this study was therefore to examine the air pressure gradient inside biofilter media as a function of the filter depth, air flow velocity, and filter material particle size distribution. The aim was to determine the shape of the pressure loss–filter depth relationship and to evaluate if present equations for predicting pressure loss are valid when taking the nonlinearity into account. Measurements of pressure loss as a function of the above parameters were carried out using a commercial biofilter packing material Leca® (Light Expanded Clay Aggregates), consisting of particles with high internal porosity (Sharma and Poulsen 2010). This material was chosen as it is available in well-defined particle sizes and that it can be taken to represent a wide range of both natural and artificial biofilter materials.

2 Theory

At low velocities, unidirectional air flow through a porous medium can be described by Darcy's law. In case of air flow, the effect of gravity is traditionally ignored as it is very small compared to the effect of velocity. In this case, Darcy's law is given as:

$$I_0 = \frac{\Delta P}{L} = \frac{\mu V}{K_a} \quad (1)$$

where I_0 is the linear pressure gradient across the medium (Pa m^{-1}), ΔP is the pressure loss across the

medium (Pa), L is the distance over which the pressure loss takes place (m), μ is the air viscosity (Pa s), K_a is the air permeability (m^2) and V is the superficial air velocity ($m\ s^{-1}$) also known as the Darcy velocity. Equation (1) is only valid when flow is laminar and inertial forces in the flow field are negligible. At higher flow velocities, when inertial forces are important, the V–ΔP relationship becomes nonlinear and Eq. (1) no longer applies. Several nonlinear equations for predicting the V–ΔP relationship in this region are available (Green and Duwez 1951; Cornell and Katz 1953; Geertsma 1979; Antohe et al. 1997; Lage et al. 1997; Trussell and Chang 1999). The most widely used is perhaps the Forchheimer relationship (Forchheimer 1901):

$$I_0 = aV + bV^2 \tag{2}$$

where a (Pa s m^{-2}) and b (Pa s^2 m^{-3}) are empirical constants that depend on the characteristics of the porous medium. Among the approaches describing fluid flow through packed beds following the Forchheimer relationship, the Ergun equation (Ergun 1952) is perhaps the most widely used. This equation is given as:

$$I_0 = A\frac{(1-\varepsilon_{tot})^2}{\varepsilon_{tot}^p}D_{eq}^{-2}\mu V + B\frac{(1-\varepsilon_{tot})}{\varepsilon_{tot}^p}D_{eq}^{-1}\rho V^2 \tag{3}$$

where A, B, and p are empirical constants, D_{eq} is an equivalent particle diameter (m), and ε_{tot} is the total fluid filled porosity (m^3 m^{-3}). Ergun (1952) proposed universal values of A, B, and p of 150, 1.75, and 3, respectively. Macdonald et al. (1979) later tested Eq. (3) against a large set of flow–pressure data from several porous media and found that A and B were dependent on medium physical properties and proposed A, B, and p equal to 180, 1.8, and 3.6 (for smooth particles) and 180, 4, and 3.6 (for rougher particles), respectively. Macdonald et al. (1991) proposed an expression for estimating D_{eq} using the first and the second order moments of the particle size distribution as:

$$D_{eq} = \left(\frac{M_2}{M_1}\right) \tag{4}$$

with

$$M_i = \int_0^\infty D_p^i n_p^i\ (D_p)dD_p \tag{5}$$

where M_i is the i'th moment, D_p^i is the particle diameter and $n_p^i\ (D_p)dD_p$ represents the number of particles with diameters between D_p^i and $D_p^i+dD_p$.

Andreasen and Poulsen (2013) measured air pressure loss in a large set of porous media with uniform particle size distributions with particle sizes ranging from 2 to 18 mm. These media were all produced from Leca®, which is a granular material used for insulation and biofiltration. Based on these measurements, Andreasen and Poulsen (2013) proposed that D_{eq}, in media with uniform particle size distributions could be estimated as:

$$D_{eq} = \frac{2}{\frac{1}{D_m} + \frac{1}{D_{min}}} \tag{6}$$

Where D_m and D_{min} are the mean and minimum particle diameters (m) for the medium, respectively. Andreasen and Poulsen (2013) further observed that the pressure loss in these media was almost independent of air-filled porosity and therefore suggested that pressure loss be predicted as:

$$I_0 = A\left(\frac{2}{\frac{1}{D_m} + \frac{1}{D_{min}}}\right)^{-2}\mu V + B\left(\frac{2}{\frac{1}{D_m} + \frac{1}{D_{min}}}\right)^{-1}\rho V^2 \tag{7}$$

Pugliese et al. (2013) tested Eq. (7) against 63 media with different particle size distributions originating from three materials with very different particle shapes and found that for Leca®: A=405 and B=50. Pugliese et al. (2013) further observed that Eq. (7) had a tendency to over predict ΔP at low and high velocities and, therefore, suggested a modified version of Eq. (7) as:

$$I_0 = A\left(\frac{1}{\frac{\alpha}{D_{10}} + \frac{1-\alpha}{D_{60}}}\right)^{-2}\mu V + B\left(\frac{1}{\frac{\alpha}{D_{10}} + \frac{1-\alpha}{D_{60}}}\right)^{-1}\rho V^2 \tag{8}$$

where α is a dimensionless weighting parameter, and D_{10} and D_{60} are the particle diameters corresponding to the 10 and 60 % fractiles of the particle size

distribution. For Leca®, Pugliese et al. (2013) suggested A=480, B=50, and α=0.7.

The theory and equations for predicting pressure loss in porous media including those described above assume that the ΔP–L relationship in a porous medium is linear (=I_0). It has long been known with respect to fluid flow in pipes that in the case of a straight pipe with constant cross sectional area cross section shape, and wall friction, the pressure decreases linearly along the direction of flow. However, presence of narrowings, expansions, or bends on the pipe causes additional pressure losses (called minor losses), thus the ΔP–L relationship along the length of a pipe with variable cross sectional area and cross section shape cannot be assumed linear. If the flow experiences a change in flow area, the biggest pressure losses are often observed at the entrance of the new flow unit. Figure 1 illustrates what happens to the fluid flow and pressure variation when entering a narrow pipe with a sharp edge. Near the entrance, the establishment of stagnant turbulent regions (vena contracta) causes an increase in fluid velocity and a rapid pressure loss. At some distance from the entrance, the velocity returns to a constant (and lower) value and the pressure gradient becomes constant. During the transition from high to low velocity, part of the pressure is regained (as momentum energy is converted to pressure).

In general, the minor losses ΔP_{minor} associated with bends, expansions, or narrowings are most commonly described as (Munson et al. 2006):

$$\Delta P_{minor} = K_L \frac{1}{2} \rho V^2 \quad (9)$$

where K_L is a loss coefficient that depends on the geometry of the flow path. Equation (9) yields the total minor pressure loss (labeled entrance loss in Fig. 1).

3 Materials and Methods

Experiments were carried out using a commercially available material, Leca®, which consists of highly porous aggregates which are nonbiodegradable, incompressible, and resistant to physical degradation. Leca® is used as an insulation or drainage material but is also finding use as filter material for a number of filtration processes including biofiltration. A view of Leca® material with different particle sizes is shown in Fig. 2.

The Leca® used in this study was supplied by Weber A/S (Randers, Denmark) in eight presorted fractions with particle size range (R) of 2 mm and particle diameters (D) of $2 \le D < 4$ mm, $4 \le D < 6$ mm, $6 \le D < 8$ mm, $8 \le D < 10$ mm, $10 \le D < 12$ mm, $12 \le D < 14$ mm, $14 \le D < 16$ mm, and $16 \le D < 18$ mm. The corresponding mean particle diameter (D_m) was 3, 5, 7, 9, 11, 13, 15, and 17 mm, respectively. From these 8 fractions, 28 additional fractions with R equal to: 4 mm (D_m = 4, 6, 8, 10, 12, 14, 16 mm), 6 mm (D_m=5, 7, 9, 11, 13, 15 mm), 8 mm (D_m=6, 8, 10, 12, 14 mm), 10 mm (D_m=7, 9, 11, 13 mm), 12 mm (D_m=8, 10, 12 mm), 14 mm (D_m=9, 11 mm), and 16 mm (D_m=10 mm) were prepared by mixing adequate amounts of eight R=2 mm fractions, yielding a total of 36 particle size fractions. All fractions were prepared so as to have a uniform particle size distribution (equal mass of all particle sizes in each fraction). Physical characteristics of the 36 Leca® fractions were determined by Andreasen and Poulsen (2013). An overview of the observed properties for the 36 fractions is given in Table 1.

Air-dry Leca® from each fraction was packed into a vertical 116-cm long, 25 cm inner diameter steel ventilation pipe to a depth of 30 cm. The pipe was fitted with a metal mesh at the bottom to support the Leca®. Thirteen small steel tubes of 1 mm inner and 3 mm outer diameter with a 1-mm opening in the center for pressure measurements were placed across the diameter of the ventilation tube. The steel tubes were located 6, 3, and 0 cm above the surface of the Leca®, at 3, 6, 9, 12, 15, 18, 21, 24, and 27 cm below the surface of the Leca® and 5.6 cm below the bottom of the Leca®. Packing was done by pouring the Leca® into prepared ventilation pipe at a constant pace to obtain an even a distribution of the material around the pressure measurement tubes as possible. When the 30 cm level was reached, the top of the medium was carefully and evenly leveled using a brush. All filter columns were prepared in triplicate yielding a total of 108 columns. Each filter was then connected to a CUBUFAN 160 EC (Jenk, Brøndby Denmark) ventilation pump, and the air was set to flow vertically down through the filter. Air flow through the medium was recorded continuously by a thermal mass flow sensor (VA400, CS instruments Tannheim Germany). A schematic of the experimental setup is given in Fig. 3.

The $\Delta P(z)$ relationship was measured for all prepared Leca® fractions at V=0.4 ms^{-1}. For selected

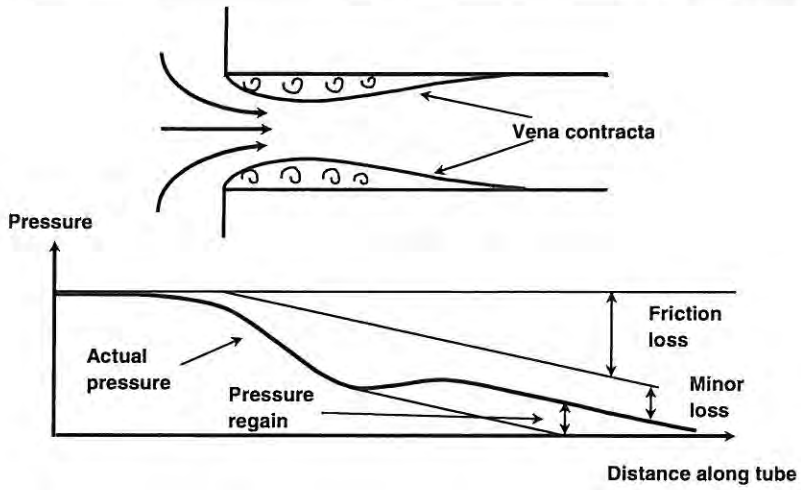

Fig. 1 Pressure variation and pressure losses associated with fluid flow from a free space into a narrow tube

fractions (2–4, 8–10, 16–18, 2–12, 6–14, 8–18, and 2–18 mm), the $\Delta P(z)$ relationship was measured for four additional values of V with the lowest equal to 0.1 ms^{-1} and the remaining three distributed evenly over the range of possible velocities for each fraction. For each fraction and velocity, the differential pressure (ΔP) between the filter outlet (the lowest steel tube) and each of the remaining steel tubes was determined when a steady-state value of V was reached, using a digital manometer (ALNOR AXD 560, Alnor, Ontario Canada). Three measurements of ΔP were taken at each measurement location for every fraction and air velocity. Average values of ΔP were then calculated for each sampling event. All measured values of ΔP values were corrected for empty column pressure loss.

4 Results and Discussion

In general, all measured $\Delta P(z)$ relationships followed the pattern indicated in Fig. 1. Data for the 10–12 mm particle size fraction at V=0.4 m s^{-1} is shown as an example in Fig. 4a. Near the inlet, the pressure inside the filter material decreases more rapidly than at larger depths where the pressure gradient approaches a constant value. This was observed for all particle size fractions and all air velocities. Together with Fig. 1, these data indicate that a pressure loss (minor loss) in addition to the constant pressure gradient that is represented by Eqs. (1) or (3) (indicated by the dotted line in Fig. 4a) takes place when the air passes from a free space (above the filter) into the porous filter medium. This minor loss is not instantaneous but takes place

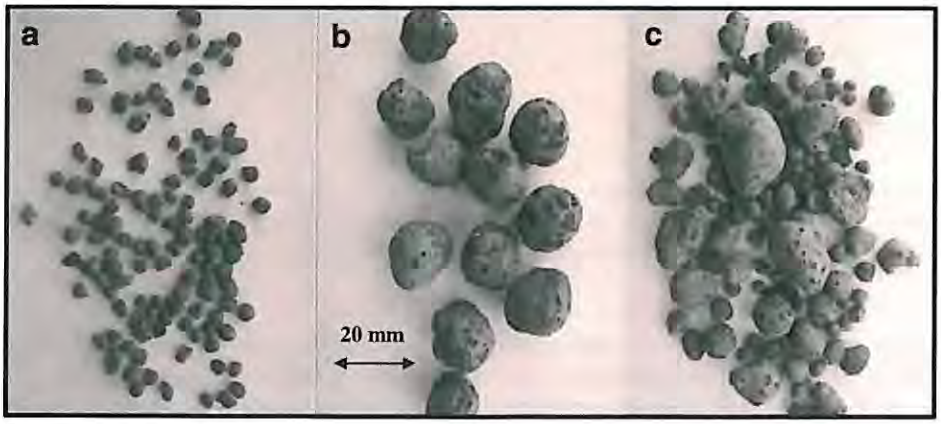

Fig. 2 Illustration of the Leca® (Light Expanded Clay Aggregates) material used in this study for producing different particle size fractions: **a** particle diameter (D) 2–4 mm, **b** 16–18 mm and **c** 2–18 mm

Table 1 Observed physical properties of the 36 Leca® particle size fractions used in this study: dry bulk density (ρ_b), particle density (ρ_p), total porosity (ϕ), external volumetric air content (ε_{ex}), and dry air permeability (k_a, dry) (Andreasen and Poulsen 2013)

Fraction (mm)	ρ_b (g cm^{-3})	ρ_p (g cm^{-3})	ϕ (cm^3 cm^{-3})	ε_{ex} (cm^3 cm^{-3})	k_a, dry (mm^2)
2–4[a]	0.33	0.46	0.87	0.28	0.04
4–6	0.29	0.47	0.89	0.39	0.14
6–8	0.25	0.40	0.91	0.37	0.29
8–10[a]	0.25	0.39	0.91	0.37	0.50
10–12	0.24	0.37	0.91	0.36	0.77
12–14	0.23	0.35	0.91	0.33	1.10
14–16	0.22	0.32	0.92	0.32	1.47
16–18[a]	0.23	0.34	0.91	0.33	1.91
2–6	0.31	0.47	0.88	0.33	0.05
4–8	0.27	0.43	0.90	0.37	0.16
6–10	0.25	0.39	0.91	0.37	0.33
8–12	0.24	0.38	0.91	0.37	0.56
10–14	0.24	0.36	0.91	0.35	0.84
12–16	0.24	0.33	0.91	0.28	1.17
14–18	0.22	0.33	0.92	0.32	1.57
2–8	0.29	0.44	0.89	0.34	0.06
4–10	0.26	0.42	0.90	0.37	0.18
6–12	0.24	0.39	0.91	0.37	0.36
8–14	0.24	0.37	0.91	0.34	0.60
10–16	0.23	0.34	0.91	0.34	0.90
12–18	0.23	0.33	0.91	0.31	1.25
2–10	0.27	0.43	0.90	0.36	0.06
4–12	0.26	0.40	0.90	0.37	0.20
6–14[a]	0.24	0.38	0.91	0.35	0.40
8–16	0.23	0.35	0.91	0.35	0.65
10–18	0.23	0.34	0.91	0.34	0.96
2–12[a]	0.27	0.41	0.90	0.35	0.07
4–14	0.25	0.39	0.91	0.36	0.22
6–16	0.24	0.36	0.91	0.35	0.42
8–18[a]	0.22	0.35	0.92	0.36	0.69
2–14	0.26	0.40	0.90	0.35	0.07
4–16	0.25	0.38	0.91	0.35	0.23
6–18	0.23	0.36	0.91	0.35	0.45
2–16	0.26	0.39	0.90	0.34	0.08
4–18	0.24	0.37	0.91	0.34	0.24
2–18[a]	0.25	0.38	0.91	0.34	0.08

[a] Indicate fractions for which pressure loss was measured for multiple air flow velocities

over some distance. The actual value of the minor loss can be determined by subtracting the measured pressure (ΔP_m) from the pressure (ΔP_0) that would exist if no minor loss was present (the dotted line in Fig. 4a). The slope of the $\Delta P_0(z)$ relationship is estimated as the slope of the linear part of the $\Delta P_m(z)$ relationship (below a depth of approximately 7 cm in Fig. 4a), and its intercept (at z=0) is at a value of ΔP_0 equal to the differential pressure well upstream of the filter (so that effects of the minor loss is negligible). The $\Delta P_0(z)$

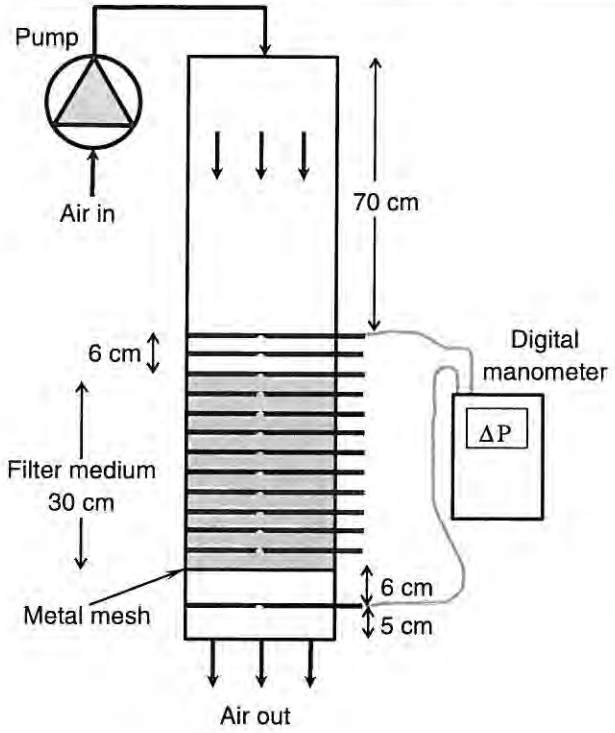

Fig. 3 Schematic of the experimental setup used in the ΔP–z measurements. *Horizontal lines* above, inside, and below the filter medium spaced 3 cm apart represent pressure measurement tubes

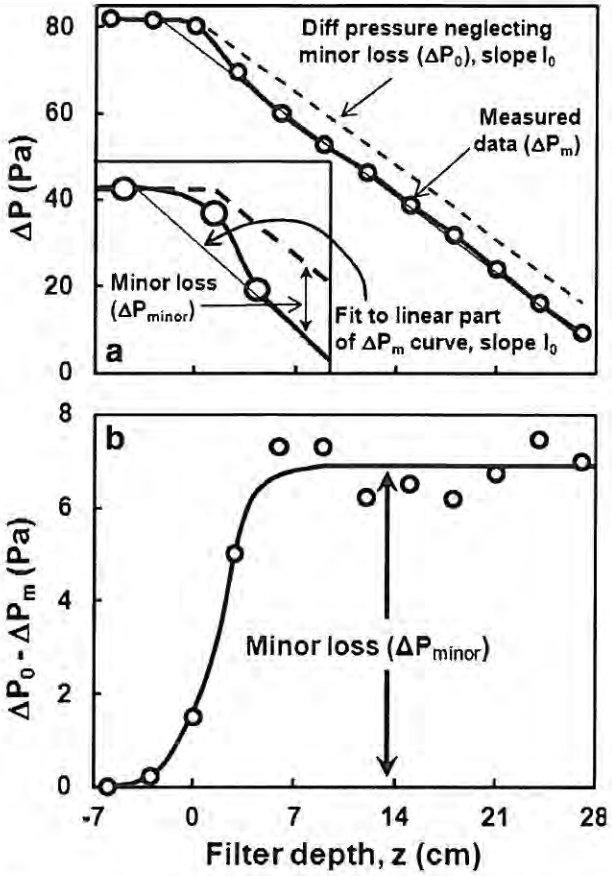

Fig. 4 Measured pressure variations and pressure losses as a function of filter depth for air flow from a free space into a porous filter material, **a** measured differential pressure (ΔP_m, symbols) and theoretical linear differential pressure (ΔP_0) assuming no minor loss (*dotted line*) as a function of filter depth. **b** Measured—theoretical (nonlinear) differential pressure difference (ΔP_0–ΔP_m)=ΔP_{minor} as a function of filter depth. *Curves* indicate the theoretical relationships. Note that ΔP_0=ΔP_i is constant above the filter inlet

and $\Delta P_m(z)$ relationships are shown in Fig. 4b. Figure 4b and the inset in Fig. 4a show that the effects of minor loss are noticeable even above the filter surface and that it takes some distance (in this case approximately 7 cm) below the filter surface before the pressure gradient stabilizes. The same behavior was also observed for all other combinations of porous medium and flow velocity. This is in essence equivalent to the behavior illustrated in Fig. 1 and suggests that flow from a free space into a porous material may be regarded as being similar to flow from a free space into several narrow tubes.

The $\Delta P_{minor}(z)$ relationships for all particle size fractions and air flow velocities investigated followed the pattern shown in Fig. 4, although there was a relatively large variation in the observed steady-state values of ΔP_{minor} and to some degree also the depth at which the steady state is achieved. It was observed that ΔP_{minor} had a tendency to decrease with increasing mean particle diameter D_m. This is illustrated in Fig. 5 that shows ΔP_{minor} as a function of filter depth for selected particle size fractions. Particle size appears to have a large influence on ΔP_{minor} but does not really affect the shape of the $\Delta P_{minor}(z)$ relationship.

For the experiments carried out in this study, the steady-state values of ΔP_{minor} are achieved below approximately 6–9 cm filter depth, constitute about 2–10 % of the total pressure loss across the filter materials considering all particle size fractions and air velocities. This is shown in Fig. 6 where values of relative inlet pressure loss calculated as $\Delta P_{minor}(z) / \Delta P_m(z = -6\text{ cm})$ as a function of filter depth for all particle size fractions and velocities considered are plotted. Considering all particle size fractions and air velocities, minor loss (ΔP_{minor}) seems to occur about 3 cm above the filter surface and increases with depth until about 6–9 cm

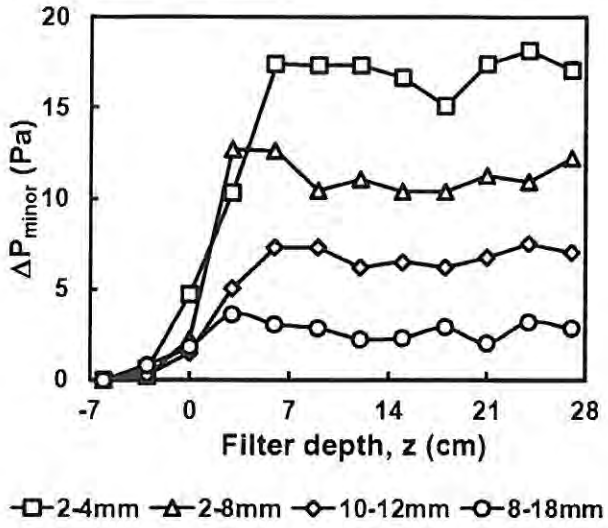

Fig. 5 Minor loss ΔP_{minor} as a function of filter depth *(z)* for four selected particle size fractions. Negative values of filter depth represent measurements taken above the inlet surface of the filter material

below the filter surface after which it becomes constant and independent of depth in agreement with Fig. 4.

The steady-state values of ΔP_{minor} were observed to increase with increasing V with most ΔP_{minor}–V relationships following a second order expression in agreement with Eq. (2), although a few are linear in agreement with Eq. (1) (Fig. 7a). For comparison, corresponding values of I_0 are plotted as a function of V in Fig. 7b. It is seen that the ΔP_{minor}–V and the I_0–V relationships generally follow the same pattern and

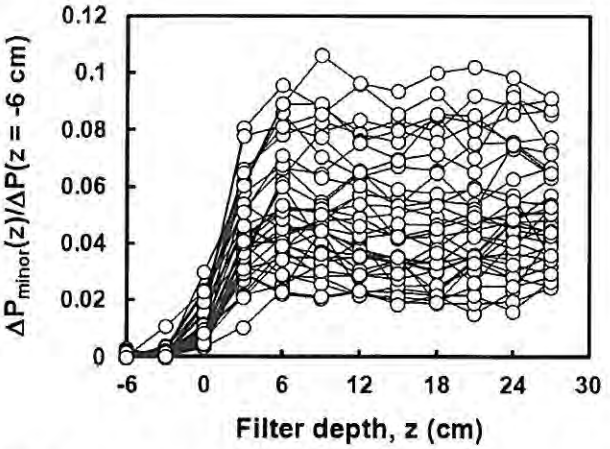

Fig. 6 Relative inlet pressure loss $\Delta P_{minor}(z)/\Delta P(z=-6$ cm*)* for 36 particle size fractions for V=0.4 m s^{-1} and 7 particle size fractions for four additional velocities yielding a total of 64 $\Delta P_{minor}(z)/\Delta P_i$ *(z=−6 cm)* relationships

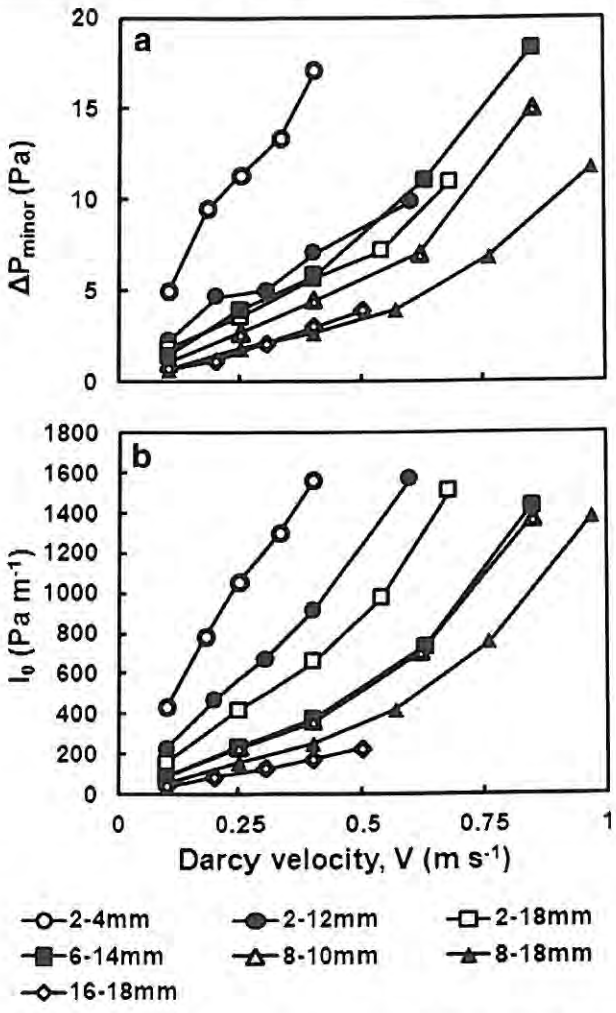

Fig. 7 **a** Minor loss (ΔP_{minor}) as a function of air Darcy velocity (V) and **b** I_0 as a function of V in selected, identical particle size fractions covering the range of particle sizes used in this study

succession (linear ΔP_{minor}–V means linear I_0–V relationships, etc.), indicating a direct proportionality between ΔP_{minor} and I_0. This is further documented in Fig. 8 that shows values of ΔP_{minor} as a function of I_0 for all 64 combinations of particle size fraction and air velocity (V). Despite some scatter in the data, it is clear that there is a relatively strong correlation between the two parameters (ρ=0.84). Figures 7 and 8 therefore suggest that ΔP_{minor} is controlled by the same material properties (e.g., particle size distribution) and operation conditions (e.g., flow velocity) as I_0.

This means that ΔP_{minor} may be predicted using the same parameters and in a similar manner as I_0, e.g., by expressions that are analogous to those proposed for predicting I_0 in earlier literature (Eqs. (7) or (8)). As

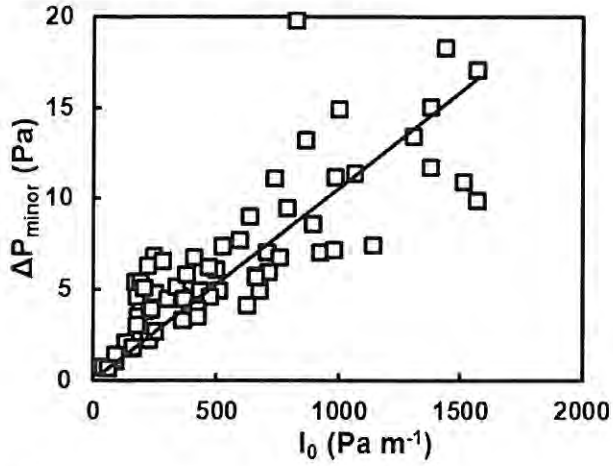

Fig. 8 Inlet pressure loss ΔP_{minor} as a function of filter pressure gradient I_0 across all 64 combinations of particle size fraction and air flow velocity. Straight line indicate the best linear fit to the data (r^2=0.64)

these equations have not been tested against V–ΔP data where effects of minor loss are accounted for, their applicability to such data was therefore evaluated by fitting them to the data measured in this study. The results are shown in Fig. 9. Resulting values of A and B for Eq. (7) were 530 and 9.2, respectively, while resulting values of A, B, and α for Eq. (8) were 890, 12, and 0.52, respectively.

The best fit is achieved using Eq. (8) with a root mean square error of 84 Pa m^{-1}, while the optimal fit of Eq. (7) yields a root mean square error of 163 Pa m^{-1}. The optimal value of α by Eq. (8) (=0.52), however, confirms that the equal weighting of the two particle diameters as also used by Andreasen and Poulsen (2013) in Eq. (7) seems valid for Leca®. As Eq. (8) yielded the most accurate fit, this model was also used as basis for calculating ΔP_{minor}. Fitted versus measured values of ΔP_i are shown in Fig. 10. Optimal values of A, B, and α were 18, 0.16, and 0.11, respectively. The measured data could be fitted with an average relative error of 38 %. It is seen that the fit is relatively good at ΔP_{minor} values below approximately 7 Pa. The reason is that there is a relatively good relationship between ΔP_{minor} and I_0 (Fig. 8) in the same region and that Eq. (8) is designed to predict I_0. Thus, a relatively good fit should be expected when using the model in this region. An explanation of the scatter in Fig. 10 is that ΔP_{minor} is essentially determined as the difference between the total pressure loss across the filter and the intercept of the best fit line to the linear part of the $\Delta P_m(z)$ relationship as illustrated in the inserted figure in Fig. 3a. As both of these are relatively large numbers while ΔP_{minor} is a relatively small number, even small uncertainties in the large numbers will cause a large relative uncertainty and thus increased scatter in ΔP_{minor}.

Despite the scatter, it is clear that the model (Eq.(8)) to some degree is able to mimic the variations in ΔP_i. Together with Fig. 7, this indicates that ΔP_i is dependent on both the particle size distribution of the porous medium and on the gas velocity. It is very likely that it also depends on other characteristics of the porous

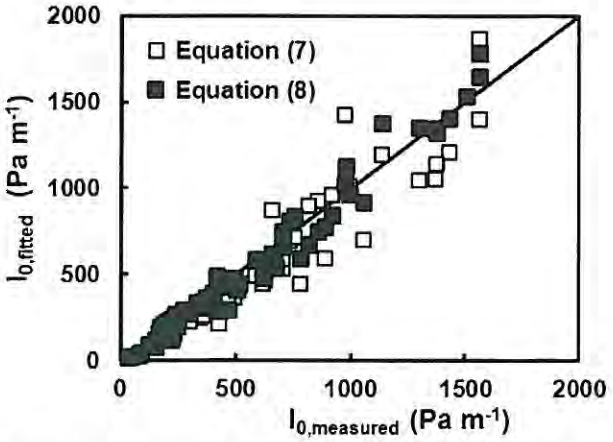

Fig. 9 Measured and fitted values of filter pressure gradient, I_0 for all 64 combinations of particle size fraction and air flow velocity using Eqs. (7) (*empty squares*) and (8) (*filled squares*)

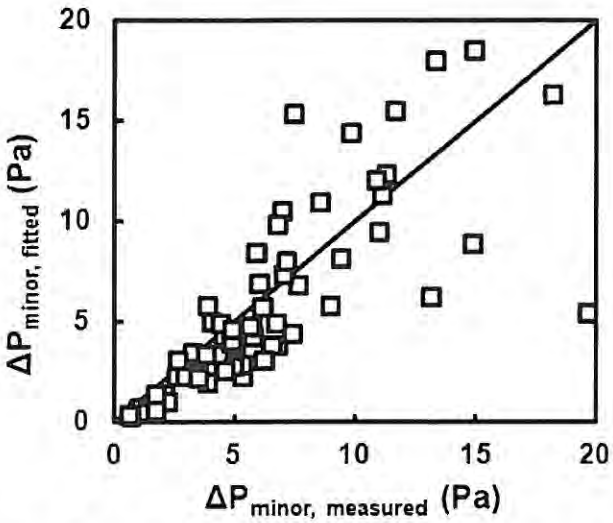

Fig. 10 Fitted (using Eq. (8)) versus measured values of ΔP_{minor} for all 64 combinations of particle size fraction and air flow velocity considered in this study

medium such as particle shape; however, more measurements are needed to verify if this is the case.

It is sometimes seen that biofilters are constructed using several filter units in series. This is done partly to ease filter irrigation and partly to facilitate control of the biological and chemical processes taking place in the filter. The results presented in this study, however, suggest that to reduce pressure loss and energy consumption in connection with the use of biofilters, it is better to use one single biofilter unit with the necessary thickness rather than several units in series (with a combined thickness equal to that of the single unit) as each of these will have the same minor loss as the single filter unit. Thus, several filters in series will have larger energy consumption than one single filter of equivalent thickness. It is noted that the use of a single filter unit may not be feasible in all cases as filter design also depends on the biological and chemical reactions taking place inside the filter, and there may be situations where it is advantageous to separate processes different filter units.

5 Conclusions

Measurements of pressure as a function of filter depth during air flow through coarse grained 2–18 mm biofilter media were conducted using several media with different particle size distributions, all originating from the same material (Leca®). These measurements revealed that the relationship between pressure and filter depth inside the filter material is not linear as normally assumed. Instead, the pressure decreased more rapidly near the filter inlet after which the pressure–depth relationship became linear at a depth of about 7 cm below the filter inlet. Thus, the pressure variation inside the filter could be described as an initial pressure loss (minor loss) occurring over the first 7 cm of the filter in combination with a linear pressure loss throughout the filter. The minor loss amounted for up to 10 % of the total pressure loss across the filter.

Two existing models for predicting pressure loss in porous media were tested against the data, and the results showed that these models could be used to calculate the linear pressure loss component with a high degree of accuracy using only a limited set of fitting parameters.

The minor loss was observed to be proportional to the slope of the linear pressure loss component, indicating that it is related to both filter medium particle size distribution and gas velocity. The existing model concept for predicting the linear pressure loss component was also applied to the minor loss and found capable of calculating the magnitude of this pressure loss with a reasonable degree of accuracy (±40 %). The models, however, are not capable of calculating the shape of the pressure loss curve in the region where the minor loss takes place.

The minor loss is essentially determined as the difference between the pressure in the filter inlet and the intercept of the best fit line to the linear pressure loss component, which are both relatively large numbers. The minor loss, however, is a relatively small number and even small uncertainties in the two large numbers will therefore cause a large relative uncertainty and therefore decreased prediction accuracy in the minor loss.

Biofilters are sometimes designed with several filter units in series to ease filter irrigation and control biological processes. If focus is solely on minimizing filter pressure loss, the results presented here suggest that it may be better to use one single biofilter unit rather than several units in series.

References

Andreasen, R. R., & Poulsen, T. G. (2013). Air flow characteristics in granular biofilter media. *Journal of Environmental Engineering, 139*(2), 196–204.

Andreasen, R. R., Nicolai, R. E., & Poulsen, T. G. (2012). Pressure drop in biofilters as related to dust and biomass accumulation. *Journal of Chemical Technology and Biotechnology, 87*(6), 806–816.

Antohe, B. V., Lage, J. L., Price, D. C., & Weber, R. M. (1997). Exper-imental determination of permeability and inertia coefficients of mechanically compressed aluminum porous matrices. *Journal of Fluids Engineering, 119*(2), 404–412.

Blanes, V., & Pedersen, S. (2005). Ventilation flow in pig houses measured and calculated by carbon dioxide, moisture and heat balance equations. *Biosystems Engineering, 92*(4), 483–493.

Cornell, D., & Katz, D. S. (1953). Flow of gases through consolidated porous media. *Industrial and Engineering Chemistry, 45*, 2145–2152.

Darcy, H. (1856). *Les fontaines publiques de la ville de Dijon*. Paris: Victor Dalmont (in French).

Datta, I., & Allen, D. G. (2005). Biofilter technology. In Z. Shareefden & A. Singh (Eds.), *Biotechnology for odor and air pollution control* (pp. 125–145). Heidelberg: Springer.

Delhomenie, M.-C., & Heitz, M. (2005). Biofiltration of air: a review. *Critical Reviews in Biotechnology, 25*, 53–72.

Deshusses, M. A. (1997). Biological waste air treatment in biofilters. *Current Opinion in Biotechnology, 8*, 335–339.

Dorado, A. D., Lafuente, J., Gabriel, D., & Gamisans, X. (2010). The role of water in the performance of biofilters: parameterization of pressure drop and sorption capasities for common packing materials. *Journal of Hazardous Materials, 180*, 693–702.

Ergun, S. (1952). Fluid flow through packed columns. *Chemical Engineering Progress, 48*(2), 89–94.

Forchheimer, P. (1901). Wasserbewegung durch boden (in German). *Zeitschrift des Vereines Deutscher Ingenieure, 45*, 1782–1788.

Geertsma, J. (1979). Estimating the coefficient of inertial resistance in fluid flow through porous media. *Society of Petroleum Engineers Journal, 1974*, 445–450.

Green, L., & Duwez, P. (1951). Fluid flow through porous materials. *Journal of Applied Mechanics, 18*, 39–45.

Lage, J. L., Antohe, B. V., & Nield, D. A. (1997). Two types of nonlinear pressure-drop versus flow-rate relation observed for saturated porous media. *Journal of Fluids Engineering, 119*(3), 700–706.

Macdonald, I. F., El-sayed, M. S., Mow, K., & Dullien, F. A. L. (1979). Flow through porous media—the Ergun equation revisited. *Industrial and Engineering Chemistry Fundamentals, 18*(3), 199–208.

Macdonald, M. J., Chu, C. F., Guilloit, P. P., & Ng, K. M. (1991). A generalized Blake-Kozeny equation for multisized spherical-particles. *AICHE Journal, 37*(10), 1583–1588.

Munson, R. B., Young, D. F., & Okiishi, T. H. (2006). *Fundamentals of fluid mechanics*. New York: Wiley.

O'Neill, D. H., Stewart, I. W., & Phillips, V. R. (1992). A review of the control of odour nuisance from livestock buildings: part 2, the costs of odour abatement systems as predicted from ventilation requirements. *Journal of Agricultural Engineering Research, 51*, 157–165.

Pugliese, L., Poulsen, T. G., & Andreasen, R. R. (2013). Gas pressure loss during transport in porous biofilter media as related to media particle size and particle shape. Manuscript to be submitted to *Journal of Environmental Engineering*.

Revah, S., & Morgan-Sagastume, J. M. (2005). Methods of odor and VOC control. In Z. Shareefdeen & A. Singh (Eds.), *Biotechnology for odor and air pollution control* (pp. 29–63). Heidelberg: Springer.

Schlegelmilch, M., Streese, J., Biedermann, W., Herold, T., & Stegmann, R. (2005). Odour control at biowaste composting facilities. *Waste Management, 25*, 917–927.

Schwarz, B. C. E., Devinny, J. S., & Tsotsis, T. T. (2001). A biofilter network model—importance of the pore structure and other large-scale heterogeneities. *Chemical Engineering Science, 56*, 475–483.

Shareefdeen, Z., Herner, B., Webb, D., & Wilson, S. (2003). Biofiltration eliminates nuisance chemical odors from industrial air streams. *Journal of Industrial Microbiology and Biotechnology, 30*, 168–174.

Shareefdeen, Z., Herner, B., & Singh, A. (2005). *Biotechnology for odor and air pollution control* . Heidelberg: Springer.

Sharma, P., & Poulsen, T. G. (2010). Gas dispersion and immobile gas volume in solid and porous particle biofilter materials at low air flow velocities. *Journal of the Air and Waste Management Association 60*, 830–837.

Trussell, R. R., & Chang, M. (1999). Review of flow through porous media as applied to head loss in water filters. *Journal of Environmental Engineering, 125*(11), 998–1006.

Yang, H., & Allen, D. G. (2005). Potential improvement in biofilter design through the use of heterogeneous packing and a conical biofilter geometry. *Journal of Environmental Engineering, 131*(4), 504–511.